Joule

CellPress

Article

A passive perspiration biofuel cell: High energy return on investment

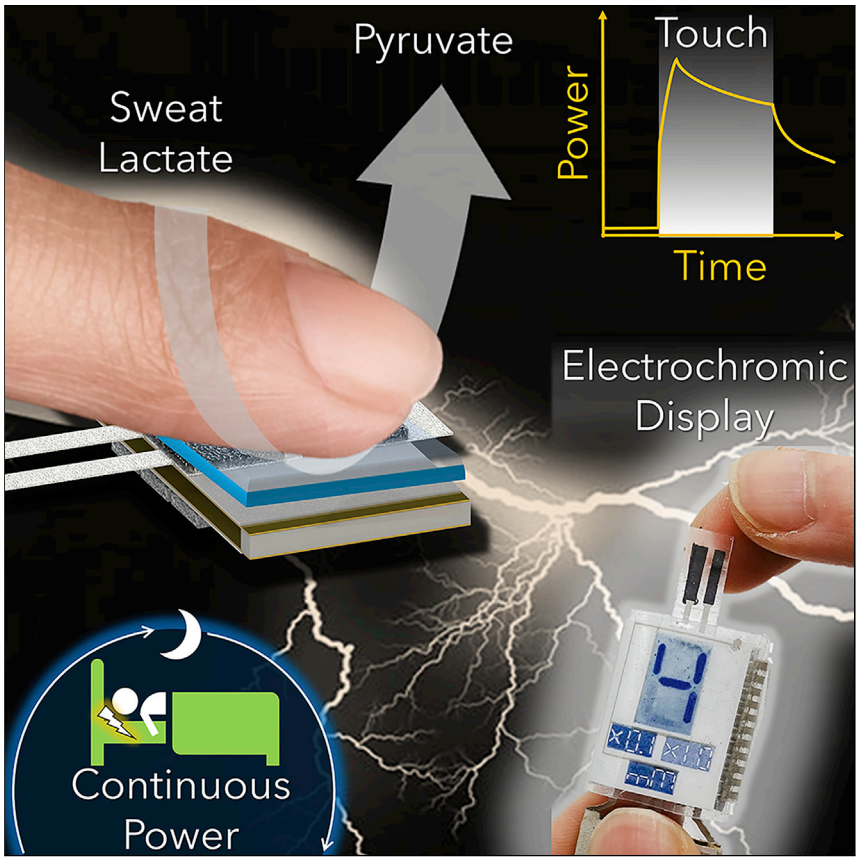

A touch-based biofuel cell that harvests bioenergy from natural perspiration and features a high energy return on investment is described. Such biofuel cells can operate continuously on a finger even without any active movement during overnight sleep and can be readily integrated with piezoelectric generators to synergistically harvest energy from fingertip pressing. The practical use of the scavenged energy is demonstrated in the powering of an integrated sensor with a dedicated display panel.

Lu Yin, Jong-Min Moon, Juliane R. Sempionatto, ..., Sang-Jin Lee, Sheng Xu, Joseph Wang

josephwang@ucsd.edu

Highlights

A novel bioenergy harvester that continuously scavenges energy from human passive sweat

Record high energy return on investment based on lactate biofuel cells

Biofuel cells harvesting ~400 mJ/cm^2 of energy during sleep without any activity

Harvesters can power an integrated sensing system with dedicated displays

Yin et al., Joule 5, 1888–1904
July 21, 2021
https://doi.org/10.1016/j.joule.2021.06.004

CellPress

Joule

Article

A passive perspiration biofuel cell: High energy return on investment

Lu Yin,[1,3] Jong-Min Moon,[1,3] Juliane R. Sempionatto,[1,3] Muyang Lin,[1] Mengzhu Cao,[1] Alexander Trifonov,[1] Fangyu Zhang,[1] Zhiyuan Lou,[1] Jae-Min Jeong,[1] Sang-Jin Lee,[1] Sheng Xu,[1,2] and Joseph Wang[1,2,4,*]

SUMMARY

Self-powered wearable systems that rely on bioenergy harvesters commonly require excessive energy inputs from the human body and are highly inefficient when accounting for the overall energy expenses. A harvester independent from the external environment for sedentary states has yet to be developed. Herein, we present a touch-based lactate biofuel cell that leverages the high passive perspiration rate of fingertips for bioenergy harvesting. Powered by finger contact, such a bioenergy-harvesting process can continuously collect hundreds of mJ of energy during sleep without movements, representing the most efficient approach compared to any reported on-body harvesters. To maximize the energy harvesting, complementary piezoelectric generators were integrated under the biofuel cell to further scavenge mechanical energy from the finger presses. The harvesters can rapidly and efficiently power sensors and electrochromic displays to enable independent self-powered sensing. The passive perspiration-based harvester establishes a practical example of remarkably high energy return on investment for future self-sustainable electronic systems.

INTRODUCTION

Wearable electronics have shown tremendous growth over the past decade.[1] Current wearable electronics are predominately powered by miniaturized electrochemical energy storage devices (e.g., batteries, supercapacitors), with limited energy and power density that cannot power the electronics over an extended operational time.[2] To address this challenge, researchers have focused on reducing energy consumption while introducing energy harvesters to offer extended system runtime.[3,4,5] Self-powered sensors that autonomously generate signals can reduce the system power consumption but cannot provide sufficient energy to the electronics for actual measurement or data transmission.[6,7] Recent progress in energy harvesters has enabled self-sustainable systems that continuously harvest energy from sunlight, movements, temperature gradients, or biofuels to power the sensors and electronics intermittently or continuously.[3,5,8–11] Unfortunately, harvesters based on an inconsistent external environment cannot supply energy on demand, while mechanical and biochemical energy harvesters require vigorous movement and with high mechanical energy investment and thus are highly inefficient, inconvenient, and lack practicality. An energy harvester relying on a passive constant input from the human body, and relying neither on irregular external environment nor movements and exercises, is therefore considered a "holy grail" of energy-harvesting devices.

Context & scale

Recent progress in energy-autonomous wearable systems requires practical and efficient energy harvesters to continuously provide power. However, most bioenergy harvesters, not relying on the external environment, are based on excessive bodily movements; only less than 1% of energy derived from the mechanical energy input can be harvested and is highly impractical and inefficient. Addressing this issue, this work reports the development of a biofuel cell that can harvest energy from the passive sweat from fingertips that can generate power continuously without any physical movement. The developed biofuel cell can scavenge ~400 mJ/cm^2 energy over 10 h during sleep and can be used to power a sensor with a dedicated display for environmental monitoring or personal wellness. Such energy harvester reports record high energy return on investment and has great implications for future high-efficiency practical energy sources for wearable electronics.

Among the aforementioned energy harvesters, lactate-based biofuel cells (BFCs) have shown considerable promise as both self-powered sensors and bioenergy harvesters for powering electronics.[3,12] Relying on the high lactate concentration in human sweat, epidermal BFCs can readily generate energy using a lactate oxidase (LOx) bioanode complemented by the oxygen-reduction reaction (ORR) on the cathode.[13] However, despite their great potential for powering wearable electronic devices, the ability to exploit the rich sweat bioenergy has been hindered by the inherent inaccessibility of natural sweat. While sweat is autonomously generated from the human body in most epidermal spaces, its flow rate is extremely low for realizing efficient bioenergy harvesting. Thus, wearable BFCs commonly require vigorous and extended exercise before a sizable amount of sweat can accumulate onto the bioelectrodes for power generation.[10] While epidermal BFCs with high power density have been reported,[3,12] the operation of such BFC-powered systems requires massive energy input toward continuous sweat generation, resulting in extremely low conversion efficiency (<1 %) when accounting for the mechanical energy input (Table S1).[10,14] Alternative approaches for accessing sweat biofuels without intensive exercise are thus urgently needed for routine and practical applications of BFCs in wearable systems.

Herein, we present the development of a high energy return on investment (EROI) harvesting device that is powered by natural, passive fingertip sweat and does not require mechanical input to instantly generate power. Different from energy-conversion efficiency, EROI describes the ratio between the harvested energy and the actively invested energy for activating the harvesters that would not be required otherwise. An extremely high EROI is critical for the long-term practicality and viability of energy-harvesting processes and should be considered critical to the development of wearable power sources toward sustainable operation of wearable electronics. We developed and optimized a BFC for collecting the natural perspiration from a finger, which is constructed with a flexible, porous, water-wicking 3-dimensional (3D) carbon nanotube (CNT) foam (Figures S1–S3 and S5; Video S1) as the BFC electrodes. The CNT foam was decorated with LOx and nanoporous Pt on the anodic and cathodic sites for lactate oxidation and oxygen reduction, respectively, for bioelectrocatalytic power generation (Figure 1A). Unlike other body locations, the sweat rate on the fingertip is considerably high (80–160 g h^{-1}).[15] Recent reports demonstrated the advantages of such fingertip natural perspiration for sweat analysis compared to common sweat simulation methods (such as exercise, iontophoresis, or heat).[16,17] Such efficient fingertip sweat generation is extremely attractive for powering BFCs without the need for sweat-inducing exercise. Porous polyvinyl alcohol (PVA) hydrogel was further employed to eliminate the Laplace pressure of sweat droplets to facilitate continuous sweat transfer from the fingertip to the BFC electrodes, while retaining the fuel toward continuous harvesting (Figures 1B and S6).[18,19] The finger contact-based BFC can continuously harvest 300 mJ/cm^2 of energy over 10 h of sleep without any mechanical input or over 30 mJ of energy per h from a single press of a finger that consumes merely 0.5 mJ mechanical energy, resulting in a high EROI of 6,000%; repeated touching results in refueling and enhanced convection, and can further boost the power to harvest more energy over a shorter time period (Figure 1C). Implementing the microgrid design concept for self-powered electronic systems,[10] this contact-based BFC has been combined with a lead zirconate titanate (PZT) piezoelectric generator to further increase the harvesting efficiency from the press of a finger, thus achieving synergistic energy scavenging (Figure 1D). As a practical application, such efficient hybrid harvesters were used to power an electronic sensing system that contains vitamin-C or sodium-ion sensors with dedicated low-power electrochromic display (ECD), to

[1]Department of Nanoengineering, University of California San Diego, San Diego, La Jolla, CA 92093, USA

[2]Center of Wearable Sensors, University of California San Diego, San Diego, La Jolla, CA 92093, USA

[3]These authors contributed equally

[4]Lead contact

*Correspondence: josephwang@ucsd.edu

https://doi.org/10.1016/j.joule.2021.06.004

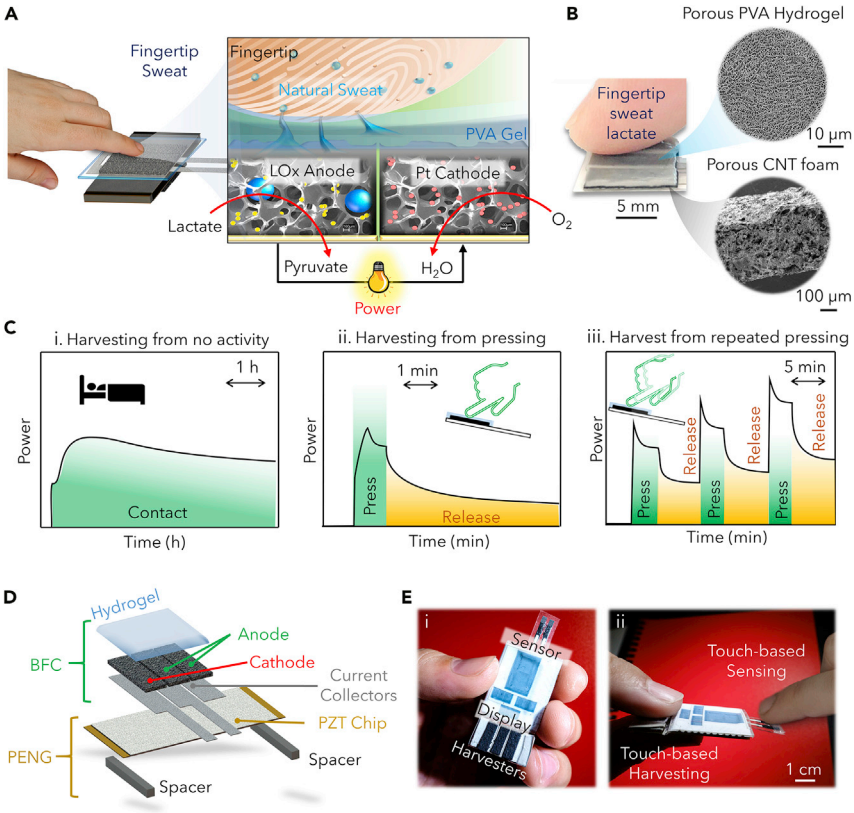

Figure 1. Schematics illustrating the operation of the touch-based BFC and bioenergy-harvesting system

(A) Schematic illustration and reaction mechanism of the BFC harvesting lactate biofuel from the natural finger sweat using LOx anode and Pt cathode.

(B) Optical and SEM images of the templated porous PVA hydrogel and CNT foam.

(C) Illustration of three operating conditions of the BFC, harvesting energy from (Ci) passive continuous contact, (Cii) active pressing, and (Ciii) repeated active pressing.

(D) Exploded view of an integrated BFC-PZT harvester to harvest chemical and mechanical energy from the press of fingers.

(E) Photo images of (Ei) self-powered sensing system with integrated harvesters, sensor, and ECD, and (Eii) device sensing sweat composition from the natural finger sweat.

See also Figures S1–S6.

operate independently from external devices (Figure 1E). Overall, the described touch-based BFC harvester demonstrates the most favorable energy EROI ever reported among all bioenergy harvesters (Table S1) and sets higher standards in the bioenergy collection efficiency of wearable harvesters. The paradigm shift from "work for power" to "live to power" greatly enhances the practicality of existing on-body bioenergy-harvesting technologies and offers possibilities for establishing reliable and independent next-generation self-sustainable electronics systems.

RESULTS

Characterization and optimization

The fabrication of a touch-based BFC that effectively utilizes soft, durable, porous, sweat-wicking CNT foam electrodes. These flexible CNT foam electrodes were prepared by using a water-soluble particle template and solvent exchange in a formulated CNT-elastomer composite. Through optimization (Figure S7; Note S1), the CNT-foam-based fingertip BFC was designed with the total size of 1 × 1 cm^2, with

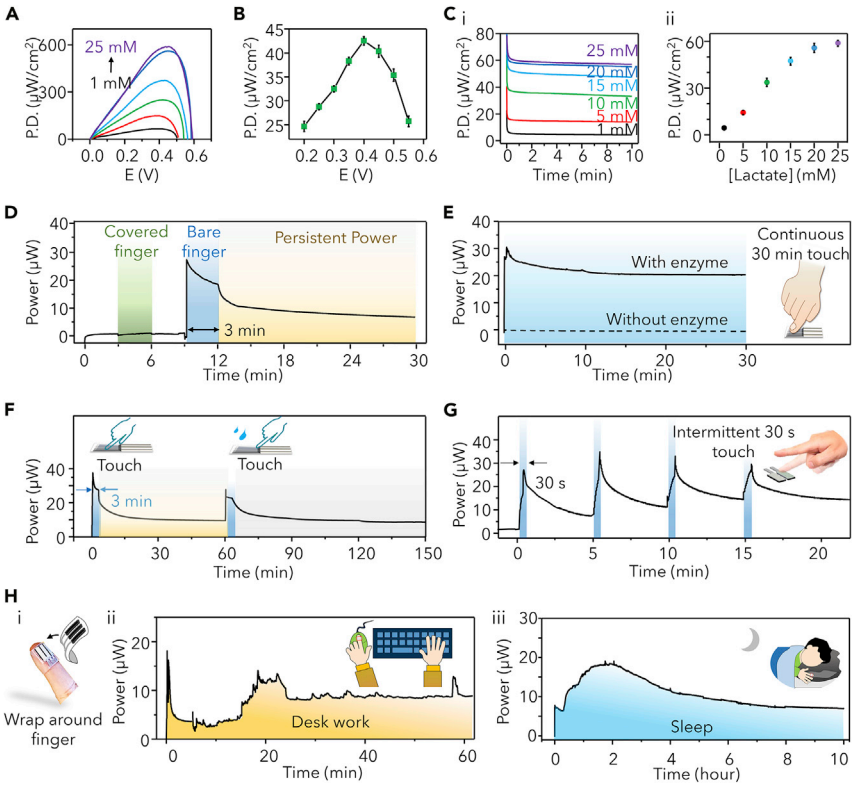

Figure 2. *In vitro* and *in vivo* characterization of the touch-based BFC

(A) Areal power density of the BFC at different lactate concentrations (1, 5, 10, 15, 20, 25 mM), characterized using LSV at 5 mV/s.

(B) The areal power density of the BFC at different potentials, characterized via 10-min CA. (Error bars: standard deviation; n = 3).

(C) (Ci) Power density of the BFC at 0.40 V in PBS with different lactate concentrations and (Cii) the power-calibration plot of the BFC with different lactate concentrations with the PVA gel. (Error bars: standard deviation; n = 3).

(D) Comparison of the power of the BFC touched by a covered finger for 3 min and by a bare finger for 3 min.

(E) Power profile of the BFC during 30-min continuous pressing, using anode decorated with and without LOx enzyme.

(F) Power profile of refueling by pressing the BFC for 3 min after 1 h of resting.

(G) Power profile of the BFC during repeated 30 s pressing every 5 min.

Note: For Figures 2D–2G, pressing pressure, 50 kPa; CA voltage, 0.40 V.

(H) (Hi) Illustration of the BFC attached to the finger for long-term continuous energy harvesting. (Hii) Power profile during a 1 h of normal desk work involving intermittent BFC pressing. (Hiii) Power profile of the BFC passively harvesting bioenergy overnight (10 h of sleep) from a finger.

See also Figures S7–S22.

one cathode electrode paired with two anodes (Figure 1B). The operational conditions of the BFC were optimized first using *in vitro* tests. The BFCs were traditionally characterized using linear scan voltammetry (LSV) with the scan rates around 5 mV s^{-1}, which was used to gauge the power of the BFC against different fuel concentrations and the peak power potential (Figure 2A). However, such a method cannot accurately depict the long-term harvesting performance in equilibrium since capacitive charging current makes up a significant part of the measured power output (Figure S10). Thus, extended chronoamperometry (CA) of 10 min was employed, with potential steps from 0.55 to 0.2 V to accurately evaluate the power and optimal operating conditions of the BFC. The open-circuit voltage of the cell demonstrated a value of ~0.55 V, in agreement with the onset potential of LOx/NQ-driven oxidative and Pt-

catalyzed reductive reactions, set at −0.2 and 0.35 V versus Ag/AgCl, respectively (Figures S8 and S9). The Pt-based ORR was chosen as a cathodic half-cell over enzymatic biocathodes to minimize the risks involved in the enzyme immobilization and to eliminate energy-harvesting fluctuations due to environmental changes. A potential of 0.40 V offered the most favorable performance with the power density of 43 μW cm^{-2} (based on the anode area) in the presence of a 15 mM lactate concentration (Figure 2B). As expected, the response of the BFC to increasing lactate concentrations, ranging from 1 to 25 mM, in both the liquid PBS and the PVA hydrogel media (under 50 kPa applied pressure), has been tested at the optimized (0.40 V) potential (Figures 2Ci and 2Cii) and led to higher bioelectrocatalytic currents. Figure 2Cii demonstrates that the PVA gel results in similar power output as the PBS buffer (Figure S12). Electrochemical impedance spectroscopy (EIS) was performed on the BFC before, after, and during application of different amount of pressure, which demonstrated low impedance of the porous PVA gel as well as to the reduced electrode resistance of the electrodes (Figure S11). The diffusion of sweat through the hydrogel was simulated by dropping 1 μL of lactate solution and observing the power profile of the BFC. As illustrated in Figure S13, this experiment shows that the diffusion time varies based on the concentration of the lactate fuel, increasing from 14 s for 20 mM droplets to 45 s for 100 mM droplets. The BFC stability was examined and showed a stable output throughout a week (Figure S14).

Figure 2D illustrates the proof-of-concept power response of the touch-based BFC. This power-time temporal profile displays a rapidly increasing power, to around 30 μW, upon pressing the BFC with a bare finger (blue section) (Video S2). In comparison, no power generation is observed for similar touching of the BFC using a finger covered by a plastic wrap (green section), reflecting the absence of fuel transfer. Such comparison clearly demonstrates that the power generation in a BFC is solely fueled by the sweat residue on the finger instead of related mechanical or thermal energy inputs from the finger. Such energy-harvesting performance was also shown to be reproducible with the same test subject, with the collected energy varying—10% among different BFC samples (Figure S15). Due to the difference in sweat rate and lactate concentration in different individuals, the harvestable power can vary from person to person, giving an advantage of BFC-produced power to individuals with higher fingertip sweat rate (Note S2; Figures S16 and S17). The harvesting behavior of BFC during continuous pressing was further validated over a 30-min period, which generated over 20 μW of power per finger and harvested over 39.5 mJ of energy over 30 min (Figure 2E). In comparison, the BFC without LOx enzyme was not able to generate any sizable energy. The ability of the touch-based BFC to continuously harvest energy from the sweat transferred from a brief (3 min) touch is demonstrated in Figure 2F, where the BFC was able to harvest energy over an hour and can be refueled upon touching the porous PVA hydrogel again. It is worth noting that without enclosure around the BFC, the collected sweat fails to maintain the hydration of the PVA gel due to faster evaporation kinetics, and the gel was required to be rehydrated with water every hour (Figure S18). As shown in Figure 2G, repeated, frequent pressing on the BFC is beneficial for increasing its harvesting power, with its power increasing after each press. Such behavior can be utilized to increase rapidly the power harvested without exerting constant force upon the device and can be further exploited with BFCs for multiple fingers to reach higher power (Figure S19). The simplicity and practicality of this touch-based BFC harvester were demonstrated in different scenarios, such as during regular desk work that involves typing and mouse-clicking (Figures 2H and S21), or during overnight sleep when no mechanical input was exerted (Figures 2I and S22). Due to the extended experiment duration, a plastic wrap was applied around the BFC to avoid hydrogel dehydration, as illustrated in Figures 2Hi and S20.

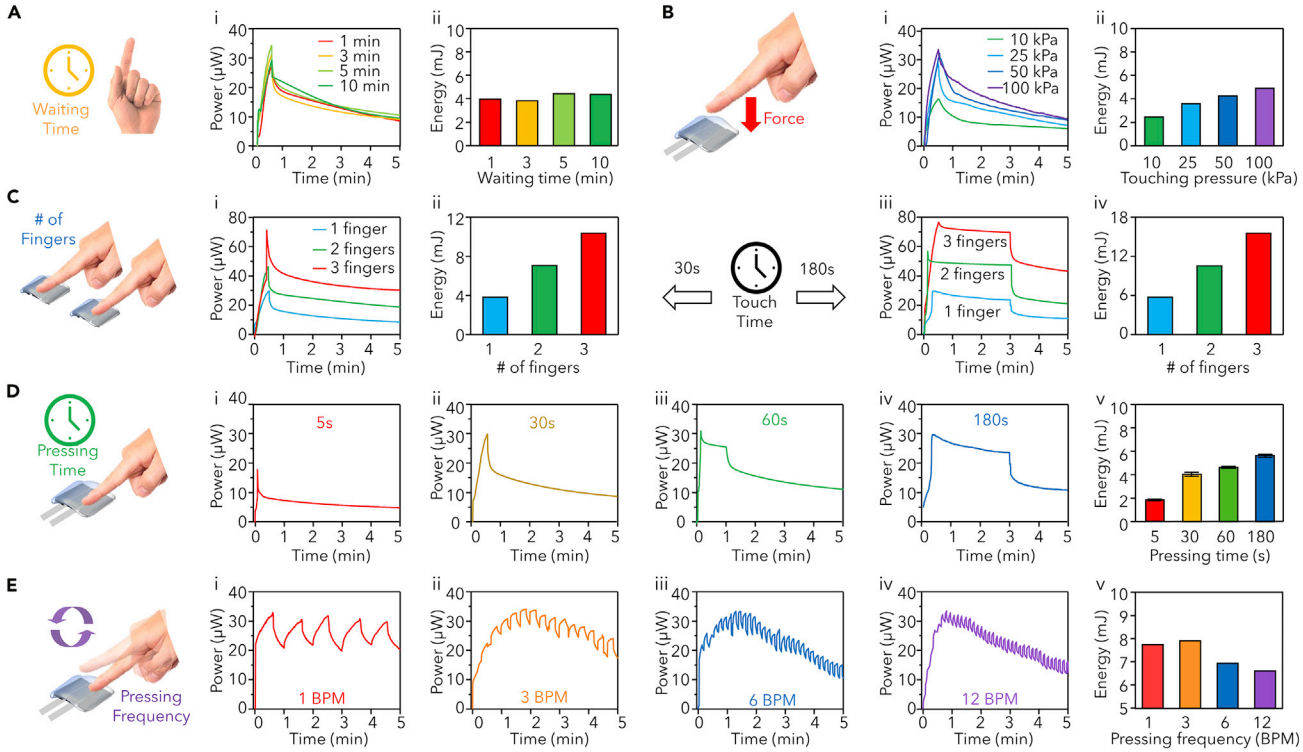

Figure 3. Optimization of the BFC usage patterns

(A) The power-generation profile and energy harvested within 5 min of the BFC touched with the pressing pressure of 50 kPa by a bare finger that has been cleaned and waited for various time periods before touching once for 30 s.

(B) The power-generation profile and energy harvested within 5 min of the BFC touched by a bare finger once for 30 s with different pressing weights.

(C) The power-generation profile and energy harvested during 5 min of the BFC touched with the pressing weight of 50 kPa by 1–3 fingers paired with a corresponding number of BFCs for (Ci) 30 s and (Cii) 3 min.

(D) The power-generation profile and energy harvested within 5 min of the BFC touched with the pressing weight of 50 kPa by a bare finger once for different time periods (5–180 s; Di–Div). (Error bars: standard deviation; n = 4).

(E) The power-generation profile and energy harvested for 5 min using different pressing frequencies with a pressing pressure of 50 kPa by one finger. See also Figures S23–S25.

These data demonstrate that the BFC can harvest energy continuously in both scenarios, scavenging over 28.4 mJ during 1 h of desk work or up to 389 mJ energy over 10 h of sleep without the need for any environmental or mechanical energy input.

To further investigate and optimize the utilization of the touch-based bioenergy-harvesting process, several variables that affect the power generation, including the sweat accumulation time (after cleaning and prior to touching), the touching pressure, the duration of touching, the number of fingers employed, and the touching frequency, have been systematically studied. Toward the practical goal of quickly powering a device within a short period after touching, the power and the total energy generated during a 5-min touching were monitored and compared. First, the effect of the sweat accumulation time before touching the BFC was examined using a 1 to 10 min time range, and the corresponding power generation was monitored during a 30-s touching time. While longer accumulation times were expected to increase the power due to the accumulation of lactate on the fingertip, no significant difference in the power was observed in the first 5 minutes (Figure 3A). Such behavior can be attributed to the constant production and reabsorption rate of sweat at a resting state,[20] which leads to a constant sweat volume and composition. On the other hand, the power difference is more pronounced through a longer operation

time of 30 min, when the stabilized power and total energy collected from the BFC increased slightly upon increasing the waiting time (Figure S23), reflecting the increased amount of fuel transfer upon touching. Subsequently, we studied the effect of the applied finger pressure on the BFC performance by touching the 1-cm^2 device with increasing pressures of 10, 25, 50, and 100 kPa. Figure 3B illustrates that a stronger press force leads to a higher power, which translates to a larger harvested energy within a fixed time. The pressure weight of 50 kPa was determined as the most appropriate since applying a larger pressure required extra effort with only negligible gain in the energy payback. It is worth noting that due to the use of the flexible and durable porous carbon-foam-based BFC and a porous PVA gel, no mechanical damage was observed throughout the process. As illustrated in Figure 3B, the power harvested from fingers is directly proportional to the number of fingers with devices deployed with different pressing duration (30 s and 3 min), where the 3-min pressing with 3 fingers harvested as high as 17 mJ over 5 min, translating to an average power of 56.7 μW and EROI of over 1,000%, considering the small amount of energy (~0.5 mJ/finger/press) used in pressing the fingers. As was shown earlier in Figure 2, pressing can increase the instantaneous power of the BFC, with the pressing time affecting the total amount of energy harvested within a short time period. As expected, the BFC pressing time profoundly affects the energy generation (Figure 3D). Such behavior shows good reproducibility in maximum power and collected energy among different BFC samples from the same test subject (Figure S24). These data display the power-time profiles recorded upon increasing the BFC touching time from 5 to 180 s. Such profiles illustrate that longer touching times lead to higher power generation and the collection of additional energy, indicating that the sweat is able to continuously diffuse through the gel during the touching period. To further examine the benefit of repeated fueling to the power harvesting within a short amount of time (toward quickly powering electronics), the 180 s touching time and the remaining 120 s idling time were divided into 5, 15, 30, and 50 segments, which correspond to touching frequencies of 1, 3, 5, and 12 beats per min (BPM), respectively. Such characterization to find the optimal pressing frequency is crucial also for further integration with piezoelectric energy harvesting nanogenerator (PENG) harvesters, which require repeated pressing for energy harvesting. As shown in Figures 3E and S25, the total energy harvested within 5 min increases to a total of 8 mJ per finger at a touching frequency of 3 BPM and starts to decrease upon raising the BPM to 12, reflecting the rapidly decreasing period when the finger was taken off from the gel.

Integrated touch-based energy harvesters

After optimizing the operation of the fingertip BFC, we evaluated the potential of the efficient bioenergy-harvesting approach toward practical autonomous and sustainable powering of wearable devices. To ensure the applicability of the self-powered device, the system is expected to store a sufficient amount of the harvested energy in a capacitor as quickly as possible, which is discharged in a burst mode to boot the electronics. To this end, the energy input from the harvesters and the energy storage capacity, as well as the system energy consumption, have to be characterized carefully along to ensure energy-budgeted, high-efficiency system operation. The energy-harvesting capability of the BFC was thus tested first via charging a capacitor that can be subsequently used for powering electronics in a pulsed manner. Due to the low potential input from the BFC, a low-power booster with energy-regulation functions was adopted to boost the BFC voltage for charging the capacitor up to 4 V. Furthermore, to fully exploit the energy input associated with the finger-pressing action, a PZT-based PENG has been integrated with the BFC in a judicious layout with a small device footprint to harvest the corresponding mechanical energy

simultaneously. Such integration allows the synergistic harvesting of bioenergy associated with the same finger-pressing motion, which requires careful considerations of the characteristics of the individual harvesters to maximize their power generation while minimizing their limitations. Due to the PENG's high alternating-voltage nature, its input was regulated via a bridge rectifier before connecting to the capacitor. The system diagram of the integrated BFC-PENG harvester is shown in Figure 4A. The PENG's energy harvesting relies entirely on the mechanical deformation of the PZT chip, located directly below the BFC energy harvester, and is activated upon finger presses. The power generated on the PZT increases upon raising the pressure, frequency, and level of deformation (controlled by the thickness of the spacer) (Figures S26 and S27). Therefore, and, as illustrated in Figure 4B, the best performance of the integrated system is expected at a touching frequency exceeding that of the BFC system alone. After the successful integration of a single set of the mechanical and biochemical energy harvesters (Figure 4Ci), an identical set of PENG harvester was attached to the opposite side of the BFC, in a sandwich-like manner, to effectively harvest the mechanical energy through a pinching motion, hence harvesting the maximum amount of power without expanding the device footprint (Figure 4Cii). Adopting the optimal pressing frequency of 6 BPM and a pressure of 50 kPa, the charging rate of one BFC without the PZT chips was tested against external capacitors ranging from 47 to 470 μF (Figure 4D). The capacitors' charging time increases upon increasing the capacitance, with the prevailing contribution of BFC as the primary energy source. To gauge the charging behavior of both types of energy harvesters, a 100-μF capacitor with a set voltage window between 2 and 4 V was used to examine their corresponding charging times. Whereas the independently acting biochemical and mechanical energy harvesters were able to charge the selected 100 μF capacitors within 8 and 20 min, respectively, the integrated system completed this task within only 4 min (Figure 4E). The contribution of individual energy harvesters shows that the amount of charge harvested by the capacitor in 2 min is the lowest for the PZT (~25 μC), moderate for BFC (~100 μC), and highest for the integrated harvesters (~125 μC). It should be noted that some synergistic behavior is expected, allowing the total harvested power to surpass the mere addition of the power from individual harvesters, as shown in Figure 4E at 4 min, where the total charge from the integrated harvesters (~220 μC) is higher than the combined BFC (~150 μC) and PZT (~40 μC). The increase in the total harvested energy can be attributed to the higher conversion efficiency of the energy regulation circuit at higher input currents and voltages.

The energy-harvesting operation was also optimized in terms of the pressing frequency of the finger. As discussed earlier, the 50 kPa pressure was found to be optimal in terms of convenience-to-power output ratio. Therefore, the influence of the touching frequency upon the bioenergy harvesting was evaluated using the 50 kPa pressure at pressing frequencies ranging from 1 to 24 BPM to determine the optimal pressing frequency that can charge the 100 μF capacitors in the shortest time. As shown in Figure 4F, a charging rate of 6 BPM pressing patterns offers faster charging of the capacitor compared to the 3 and 12 BPM pressing frequencies and leads to the fastest charging speed. The trend observed in Figure 4F is in agreement with the profiles shown in Figure 4B, as the lower frequency (3 BPM) provided less mechanical energy input for the PZT, while the higher charging frequency reduces the biochemical energy-harvesting efficiency for the BFC (Figure 3E), leading to an optimal charging rate at 6 BPM with the lowest charging time. With the optimized pressing frequency of 6 BPM, we compared the performance of a single BFC harvester to its sandwiched configuration (two back-to-back integrated devices) (Figure 4G). As expected, the double-sided harvesting device, employing two fingers' pressing motions for energy harvesting at

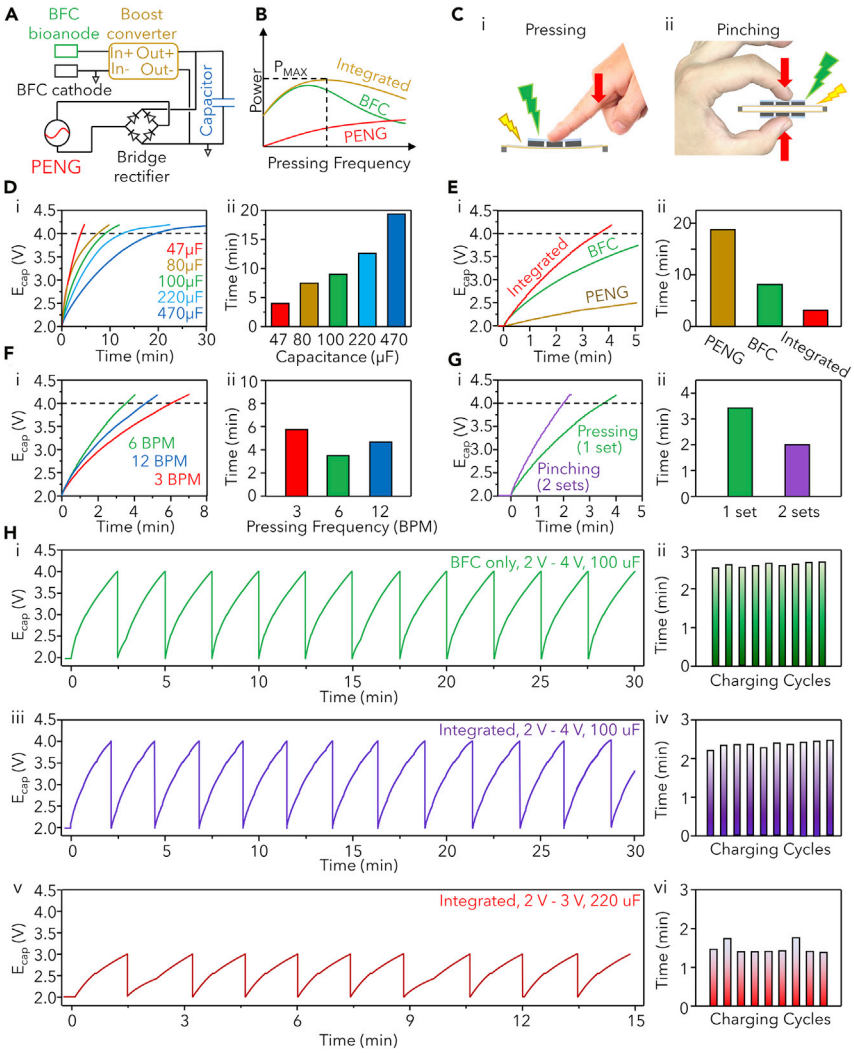

Figure 4. Performance of the touch-based BFC and the integrated harvesting system

(A) System diagram of the integrated BFC-PZT touch energy-harvesting system.

(B) Illustration of finding the optimal energy-harvesting operation setup.

(C) The two modes of operation based on (Ci) pressing with 1 finger with 1 set of integrated harvesters and (Cii) pinching with 2 fingers and 2 sets of integrated harvesters in a sandwich configuration.

(D) One BFC harvester pressed with 6 BPM frequency (Di) charging capacitors with different capacitance and (Dii) their corresponding charging times.

(E) (Ei) The charging of a 10-μF capacitor using only one PZT harvester, one BFC harvester, and one integrated harvester pressing at 6 PBM frequency and (Eii) their corresponding charging times.

(F) (Fi) The charging of a 100-μF capacitor using one integrated harvester pressing at different frequencies and (Fii) their corresponding charging times.

(G) (Gi) The charging of a 100-μF capacitor using only one and two sets of integrated harvesters pressing at 6 PBM frequency and (Gii) their corresponding charging times.

(H) (Hi) The charging of a 100-μF capacitor from 2 to 4 V (Hi) using only two BFC harvesters pressing at 6 PBM frequency, and (Hii) their corresponding charging times; (Hiii) using two integrated BFC-PZT harvesters pressing at 6 BPM and (Hiv) their corresponding charging times. (Hv) The charging of a 220-μF capacitor from 2 to 3 V using two integrated BFC-PZT harvesters pressing at 6 BPM and (Hvi) their corresponding charging times.

See also Figures S26–S28.

6 BPM, charges the 100 μF capacitors to 4 V within about 2 min, compared with the 4 min-charging time observed with the single PZT-integrated BFC setup. Lastly, the continuous energy-harvesting ability of the double-sided BFC-PZT was examined at the previously optimized conditions (50 kPa at 6 BPM). As shown in Figures 4Hi and 4Hii, two sets of BFC harvesters can effectively and consistently charge the capacitor in every ~2.8 min over the 30 min period. Similarly, the integrated BFC-PZT harvester pair also delivered consistent energy production, offering a faster charging time of ~2.3 min (Figures 3Hiii and 3Hiv). The charging process was also tested on a subject with a lower sweat rate, which results in a slight increase in the charging time (Figure S28). Furthermore, in order to further reduce the charging time of the system, a similar amount of charge can be harvested at a lower voltage by employing capacitors with larger capacitance. As shown in Figures 4Hv and 4Hvi, a 220-μF capacitor was charged in the voltage window between 2 and 3 V, which takes only ~92 s, and is significantly faster compared with charging the 100-μF capacitor to 4 V. Such change can be beneficial to the rapid powering of electronic devices, and the lower voltage can also limit the power consumption of the microcontroller unit (MCU) (Figure S31). The PZT-integrated sandwiched BFC system was shown to be the most efficient, continuously and repeatedly charging the capacitor followed by its polarization. The integrated system allows substantial energy harvesting using the pinching motion and natural sweat flow with negligible energy input. Considering the energy input of pressing the fingers every 10 s (~1 mW), such energy-harvesting behavior is attractive compared with the typical tribo/piezoelectric harvesters and BFCs that require movements or exercise as energy input (>100 W).[21,22] These results exemplify the potential of the hybrid BFC-PZT harvesters' integration for practical applications, demonstrating the most favorable EROI ever reported among all bioenergy harvesters and setting higher standards in the bioenergy collection efficiency of wearable harvesters.

Self-powered sensing system

To demonstrate the practical utility of the finger-based integrated bioenergy harvester for powering electronics, a potentiometric sensing system with an ECD panel, operated in pulsed sessions, was developed (Figure 5A). Such a system is composed of the energy-regulation components that separately manage the low-voltage, continuous input from the BFCs via a booster circuit and the high-voltage, alternating, and pulsed input from the PZT chips via a bridge rectifier (Figures 5B, S29, and S30). Both rectified energy inputs are collected in a capacitor. The overvoltage protection function of the booster was utilized, which was connected to an analog switch that controls the supply of energy to the MCU from the capacitor. A low-power MCU with a 10-bit analog-to-digital (ADC) resolution was chosen to read the voltage input from the sensor and control the "on" and "off" of 10 individual ECD pixels (Video S3). The ECD, fabricated via layer-by-layer screen-printing (Figures 5Ci and S34), was chosen for its low energy consumption, as it required energy only while refreshing the displaying content. The pixels contain a 7-segment numerical display, along with two pixels for displaying the range ("×0.1" and "×10") of the sensing and one pixel displaying "mM" as the unit of the chemical sensing when the system boots for the first time (Figures 5Cii and S35). The system design obviates the integration of any wireless communication electronics, as such systems would require external electronics (e.g., smartphone, smartwatch, computers) for data transmission and processing the sensing results. To maximize the efficiency of the system while ensuring the ECD operation, the power and charge consumption for the MCU and the ECD were carefully characterized, the capacitance for energy storage was optimized at 220 μF, and the operation window of 3 to 2 V (Note S4; Figures S31–S33 and S36). Two sets of integrated BFC-PZT harvesters, configurated back-to-back, were connected to the system to supply the harvested biochemical and mechanical energies from the pinching motions of the thumb and the index finger. Sensors can

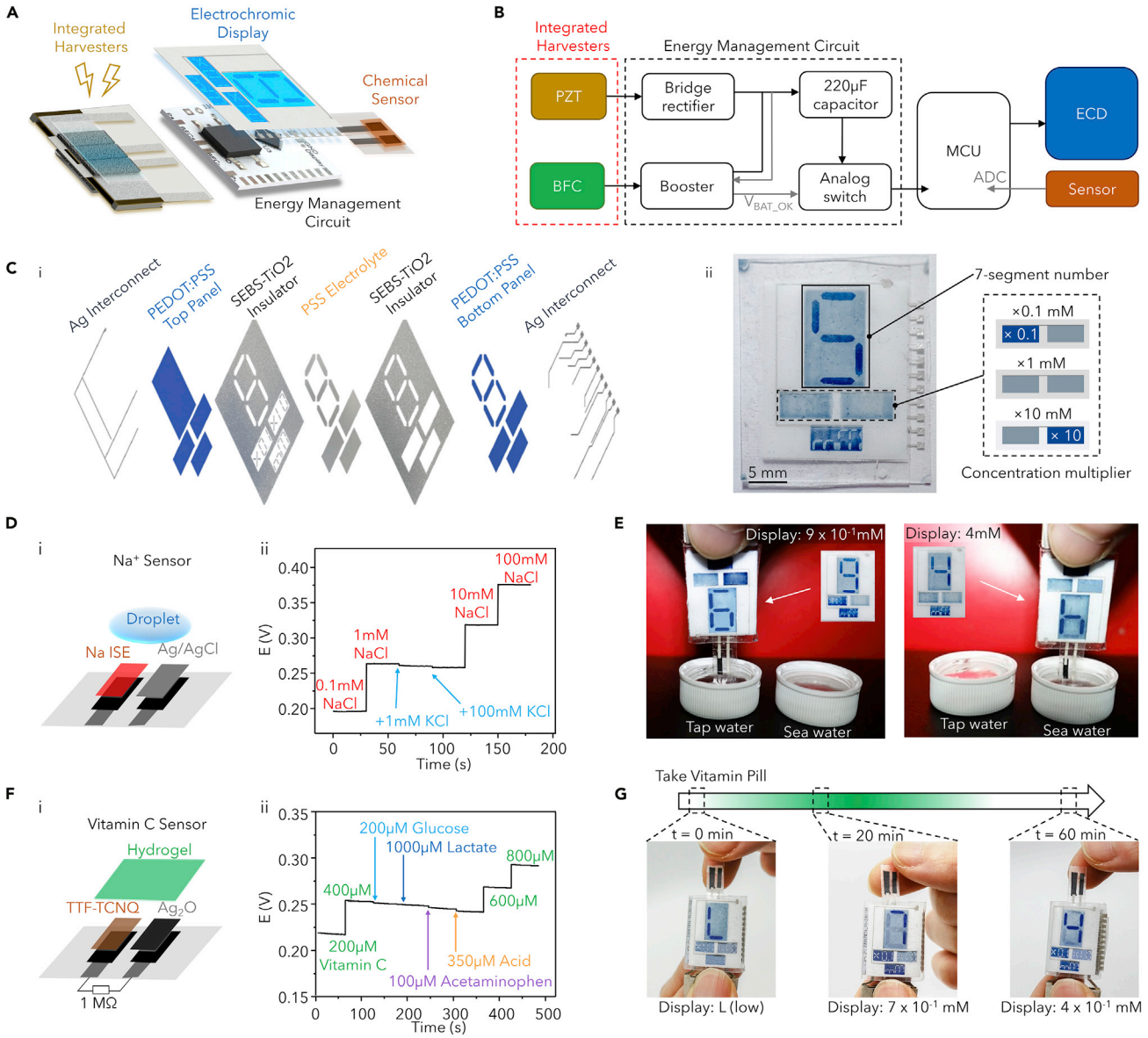

Figure 5. Operation of a self-powered sensor-display system

(A) Exploded view of the device schematics including two pairs of BFC-PZT harvesters, 2-electrode sensor, ECD panel, and related MCU and power-management circuit.

(B) System diagram of the self-powered system.

(C) The low-power ECD in (Ci) exploded view schematics and (Cii) illustration of the readings on the display panel.

(D) (Di) Illustration of the 2-electrode ion-selective sodium sensor, and (Dii) the calibration and selectivity of the sodium sensor.

(E) Photos of the self-powered sensing system, detecting sodium concentration in tap water and 1:100 diluted seawater.

(F) (Fi) Illustration of the 2-electrode vitamin-C sensor and (Fii) the calibration and selectivity of the vitamin-C sensor.

(G) Timescale of the vitamin-C testing after taking a vitamin pill (top) and corresponding photo images of the ECD reading at different times after taking the pill, tested using the self-powered sensing system.

See also Figures S29–S40 and Tables S2 and S3.

be connected to the system ADC channel for data acquisition, and the results are displayed via the ECD in the resolution of 1 significant figure (Tables S2 and S3).

Two types of sensors were employed for demonstrating the applicability of such a self-powered sensing system: a potentiometric sodium sensor and a vitamin-C

sensor. The potentiometric sodium sensor relies on measuring the potential difference between the sodium-ion-selective membrane on the working electrode and the silver/silver chloride (Ag/AgCl) reference electrode when in contact with the sodium sample solution (Figure 5Di). The electrode-electrolyte interface results in a sodium concentration gradient (between the membrane and the solution) leading to a potential signal that depends logarithmically on the sodium concentration.[23] Such potentiometric sensing applies to a wide range of clinically or environmentally important electrolytes. Figure 5D depicts the calibration of the fabricated sodium sensor, demonstrating a slope of 59.3 mV per decade of sodium concentration. It also indicates a good selectivity against potassium ions, which displays a negligible change in the sensor potential. As shown in Figure 5E, the system can boot upon pressing the energy harvesters monitoring different sodium concentrations in tap water and 1:100 diluted seawater.

Vitamin-C sensing commonly relies on amperometric measurements converted here into potentiometric ones via a controlled load. Such sensors, usually referred to as "self-powered" sensors, are based on the autonomous oxidation reaction on the working electrode along with a complementary reduction reaction on the counter electrode, analogous to those of BFCs (e.g., enzymatic glucose, lactate, or alcohol sensors). In this case, the sensing principle is based on electrocatalytic oxidation of the vitamin, generating a proportional current flow, which is further converted into a potential difference signal (ΔE) under the applied load.[24,25] The vitamin-C sensor relies on the selective, non-enzymatic oxidation of ascorbic acid (AA) on the anode catalyzed by the immobilized tetrathiafulvalene-tetracyanoquinodimethane (TTF-TCNQ) charge-transfer complex; silver oxide (Ag_2O), which delivers a stable potential throughout its reduction, was used as the cathode material (Figure 5Fi). The sensing of vitamin C in stimulated sweat was described previously and was adapted here to detect the vitamin C levels in the natural fingertip sweat (**Note S5**).[26,27] The load between the two electrodes was optimized at 10 MΩ. The calibration experiment in Figures 5F and S38 demonstrates the sensitivity of the vitamin-C sensor, while the corresponding interference study illustrates the high selectivity of the sensor against common sweat constituents, including glucose, urea, lactate, and acetaminophen. For this, a hydrogel, similar to that used in the BFCs, was presoaked in artificial sweat and placed over the sensor to absorb the fingertip sweat upon touching. The on-body usage of the touch-based vitamin C sensing was optimized for sweat generation time (60 s) and sweat collection time (120 s) (Figure S39). A human subject was asked to take a vitamin pill and sense the vitamin C level continuously over 30 min (Figure 5G). The ECD can quickly update the resulting vitamin C concentration (every 1 to 2 min), and the sensing system was able to capture the dynamics of the rise and fall of the vitamin C concentration within the natural fingertip sweat (Figure S40). Unlike other studies that use various energy harvesters for self-powered sensing and require rapid movements and rigorous exercises, the present system can boot rapidly and continuously, and efficiently harvest energy from the slow pressing action of fingers and effortlessly supply power to complex electronic systems. Thus, the integrated harvesting system has shown its distinct advantage in practical application as an independent, self-powered electronics system for personalized health and nutrition wellness or environmental monitoring.

DISCUSSION

In this work, we have demonstrated a biofuel energy harvester with extremely high EROI, which effectively harvests energy from natural fingertip sweat and the fingers'

pressing motion and its practical application in a self-powered and fully integrated sensing device. The demonstrated concept utilizes continuous naturally pumped sweat and intuitive finger pinching motions for energy generation and the operation of low-power electronics and shifts the current paradigm of bioenergy-harvesting devices from "work for power" into "live to power." This concept was demonstrated by energy harvesting during sleep or low-intensity desk work, converting traces of kinetic and chemical energies resulting from our daily activity into electric form. Utilizing the effortless and continuous fingertip sweating as the energy source, the BFC harvester is further boosted by a piezoelectric PZT harvester that fully exploits the intuitive finger motion of pinching. With a small footprint of 2 cm^2, this system delivers similar energy-collection performance while exhibiting a high energy-harvesting efficiency compared with previously reported bioenergy harvesters, which require vigorous motions or extreme sweat-inducing exercise. Pairing a low-power ECD with the touch-based harvester platform presented an energy-efficient electrochemical sensing system that can be applied to a wide variety of sensors for personalized health and nutrition-monitoring applications, beyond the demonstrated sweat vitamin C and sodium sensors.

The integrated system has been designed around smart and highly efficient utilization of limited bioenergy to realize a fast-responding, extended, and autonomous operation in connection to complementary, synergistic harvesters, optimized energy storage units, low-power energy management integrated circuits, MCUs, and displays. Future efforts will be directed toward further improvements the efficiency of the bioenergy-harvesting device and its integration with other scenario-specific harvesters. The possibility of utilizing passive sweat for a self-powered sensor whereby the sensor's power or open-circuit voltage can serve as the signals proportional to the sweat analyte concentration[13,28] can also be explored. Attention will also be given to optimizing the porous, sweat-wicking current collectors and hydrogel for better durability and moisture retention under extended, repeated operation. Such highly efficient, user-friendly, biocompatible energy-harvesting technology, coupled with the system integration and corresponding judicious energy budgeting, offers considerable promise for establishing self-sustainable, reliable, and independent next-generation epidermal electronics systems for tracking healthcare and wellness.

EXPERIMENTAL PROCEDURES

Resource availability

Lead contact

Further information and requests for resources and materials should be directed to and will be fulfilled by the lead contact, Joseph Wang (josephwang@ucsd.edu).

Materials availability

This study did not generate new unique materials.

Data and code availability

The data of this study are available from the authors upon reasonable request.

Chemicals

Graphite, toluene, sodium bicarbonate ($NaHCO_3$), acetone, ethanol, hydrochloric acid (HCl), copper sulfate pentahydrate ($CuSO_4$), 1-ethyl-3-(3-dimethylaminopropyl)carbodiimide (EDC), N-hydroxysuccinimide (NHS), 1,4-naphthoquinone (NQ), chitosan, glutaraldehyde, acetic acid, nafion, lactatic acid, silver (Ag) flakes, Ag_2O powder, PVA, potassium hydroxide (KOH), titanium dioxide (TiO_2), sodium ionophore X, sodium tetrakis[3,5-bis(trifluoromethyl)phenyl]borate (Na-TFPB),

bis(2-ethylhexyl) sebacate (DOS), tetrahydrofuran (THF), polyvinyl butyral (PVB), sucrose, sodium chloride (NaCl), methanol, iron(III) chloride ($FeCl_3$), sodium polystyrene sulfonate (PSSNa), glycerol, D-sorbital, acrylamide, N,N′-methylenebisacrylamide, sodium peroxydisulfate, and dodecyl benzene sodium sulfonate were all purchased from Sigma Aldrich. The polyurethane (PU) (tecoflex EG-80A) was obtained from Lubrizol. SEBS (G1645) triblock copolymer was obtained from Kraton. The carboxylic acid functionalized multiwall carbon nanotube (MWCNT-COOH) was purchased from Cheap Tubes. The printable poly(3,4-ethylenedioxythiophene): polystyrene sulfonate (PEDOT:PSS) screen-printable paste was purchased from Sun Chemical. The lactate oxidase (LOx) was purchased from Toyobo. The platinum electrodeposition solution was purchased from Technic. The CapstoneTM fluorosurfactant FS-65 was purchased from DuPont. The PZT discs were purchased from APC International and trimmed into 2 × 1 cm^2 chips. All electronics components were purchased from Digikey. All electrochemical measurements were performed on Autolab PGSTAT204 potentiostat/galvanostat from Metrohm.

Fabrication of the flexible CNT foam

The fabrication procedure of the flexible CNT foam is described in Figure S1. In detail, MWCNT-COOH (0.25 g), graphite (0.05 g), and $NaHCO_3$ (6.0 g) were mixed well with a motor and pestle to obtain gray-colored powders, followed by adding 3.0 g of SEBS (dissolved in toluene with 4 (SEBS):10 (toluene) wt %) and stirred at 1,800 rpm for 5 min. Subsequently, 2.5 ml of toluene was added and mixed again at 1,800 rpm for 5 min to attain a homogeneous paste. The resulting paste was then cast in 1 mm high rectangular-shaped structure, carefully controlled by placing two glass slides (1 mm thick) with controlled spacing in between. Immediately, the cast portion was transferred to ethanol for 20 min for solvent exchange that prevents collapse of the SEBS composite structure during evaporation of the solvent (toluene) and then dried in ambient conditions. After that, the dried CNT foam was soaked in 0.5 M HCl for 3 h to completely remove the $NaHCO_3$ template; this process resulted in the highly porous CNT foam structure. The resulting porous CNT foam was washed with distilled water for several times and dried at 80°C to obtain flexible CNT foam.

Fabrication of the biofuel cell

Each CNT foam was cut into 0.3 cm^2 (1 cm × 0.3 cm) and two of them (for anodes) were immersed in 10 mM EDC/NHS solution for 6 h to activate the carboxylic acid groups of the MWCNT. After washing the CNT foams with DI water several times, they were attached to the silver current collector with carbon ink placing the cathode between the two anodes. Each bioanode was fabricated by drop-casting 10 μl 0.2 M NQ (dissolved in 1:9 ratio of acetone: ethanol), followed by the addition of LOx (40 in 10 mg ml^{-1} of BSA, 10 μL) for 3 h. For immobilizing the enzyme, 5 μl each of 1% chitosan in 0.1 M acetic acid and 1% glutaraldehyde were drop cast on the anode then kept at 4°C overnight. Otherwise, the cathode was fabricated by a fixed-potential co-electrodeposition of Pt and Cu at −0.75 V for 600 s followed by de-alloying the Cu with cyclic voltammetry over the potential range of 0 to 1.5 V for 40 cycles (scan rate 50 mV s^{-1}). After rinsing with DI water several times, 2.5 μl of a 1% Nafion solution was drop cast on the cathode and kept at room temperature until use.

Fabrication of the porous PVA hydrogel

The fabrication of the porous PVA hydrogel was adapted from previous studies.[29] First, solutions of the PVA dissolved in water in a 1:10 weight ratio and KOH dissolved in water in a 1:5 weight ratio were prepared. Then, 14 g of the KOH solution was added dropwise to 10 g of PVA solution with stirring, followed by dissolving 2.6 g of sucrose into the mixture to form the hydrogel precursor. 15 g of the precursor was then poured into a

Petri dish (diameter ~9 cm) and left in a vacuum desiccator to remove excess water and allow crosslinking until only 1/3 of the weight of the precursor was left. The crosslinked gel was then soaked in 0.1 M PBS buffer to remove the sucrose template and the excess KOH, until the gel is in neutral pH. The gel can then be cut into desired sizes and shapes and stored in PBS or AS for subsequent use.

Fabrication of the electrochromic display

The ECD was designed using AutoCAD and screen-printed layer-by-layer onto SEBS sheets. The design of the ECD was separated into a front panel and a back panel, which were separated by a layer of a white, opaque insulator and PSSNa electrolyte, and assembled via heat sealing. The detailed process was described in the Note S3.

Fabrication of the sensors

The sodium sensor was fabricated using flexible silver and carbon inks based on the previous studies.[10] The silver ink and the carbon ink were printed onto SEBS substrate layer-by-layer and were covered using SEBS resin to define the electrode area, exposing 2 mm^2 of carbon electrode as the working electrode and 1 mm^2 of the silver electrode as the reference electrode. A 0.1 M $FeCl_3$ solution was first drop cast onto the silver electrode to chlorinate the surface and form AgCl.

A cocktail composed of PVB (78.1 mg ml^{-1}), and an excess amount of potassium chloride (50 mg ml^{-1}) dissolved in methanol was drop cast onto the chlorinated surface (1.5 μl mm^{-2}). A PU resin (1 g in 10 g THF) was then drop cast onto the dried cocktail layer (2 μl mm^{-2}) to prevent salt leaching. A cocktail for the sodium ion-selective electrode was formulated by dissolving 1 mg of sodium ionophore X, 0.77 mg Na-TFPB ion exchanger, 33 mg PVC, and 66 mg DOS in 660 mL nitrogen-purged THF, and drop cast onto the carbon electrode (2 μl mm^{-2}).

The vitamin C sensor was fabricated using flexible silver, carbon, and silver oxide inks.[30] The inks were printed layer-by-layer onto a SEBS substrate and covered using SEBS resin to define the electrode area, exposing 2 mm^2 of carbon electrode and 4 mm^2 silver oxide electrode. A 10 MΩ resistor was solvent-welded between the two electrodes as the discharging load. A 5 mM solution of TTF-TCNQ, dissolved in ethanol: acetone (1:1) mixture, was drop-casted onto the carbon electrode (1 μl mm^{-2}), followed by drop-casting a 1 μl mm^{-2} chitosan layer (1 wt % in 0.1M acetic acid) and a 0.125 μL mm^{-2} glutaraldehyde layer (0.5% in water) for immobilization.

The detailed fabrication process of the sensors was described in the Note S5 and Figures S37–S40.

Electrical circuit design

The circuit was composed of four main components: the MCU (AtTiny 441, Microchip Technology, USA), the analog switch (MAX4715EXK+T, Maxim Integrated, USA), the booster (bq25505, Texas Instruments, USA), and the bridge rectifier (DF02S, ON Semiconductor, USA). The PCB was designed using Altium designer and was manufactured by JLCPCB. The PCB design is illustrated in Figure S30. Individual components were then soldered onto the PCB via a standard reflow process. The integrated circuit could perform energy harvesting, storage, and power management. The MCU with a built-in ADC could read from the sensor and display the corresponding result via the ECD.

Assembly of the self-powered sensing system

An adaptor that connects two sets of BFCs and PZT chips were designed using AutoCAD and screen-printed onto a SEBS sheet (Figure S4). The front and the back PZT

chips were separately connected to the adaptor and the two PZT chips were placed back-to-back, separated by two spacers (1 mm thick) place on two ends of the chips. The foam BFC electrodes were thereafter fixed onto their corresponding locations using conductive carbon ink and modified using the procedure above. The connector was then connected to the PCB via the "solvent welding process" following previous studies.[31] Similarly, the display and the sensor was connected to the PCB using the same process to complete the assembly of the self-powered sensing system.

SUPPLEMENTAL INFORMATION

Supplemental information can be found online at https://doi.org/10.1016/j.joule.2021.06.004.

ACKNOWLEDGMENTS

This work was supported by the UCSD Center for Wearable Sensors. J.-M.M. acknowledges the support from the National Research Foundation of Korea (NRF-2019R1A6A3A12033345). We would like to thank Kraton for supplying the Styrene-ethylene-butylene-styrene (SEBS) used in this work.

AUTHOR CONTRIBUTIONS

Conceptualization, L.Y., J.-M.M., and J.W.; methodology, L.Y., J.-M.M., and J.R.S.; software, M.L. and Z.L.; validation, L.Y., J.-M.M., and J.R.S.; formal analysis, L.Y., J.-M.M., and J.R.S.; investigation, L.Y., J.-M.M., J.R.S., M.L., M.C., A.T., F.Z., Z.L., J.-M.J., and S.-J.L.; resources, S.-J.L. and J.W.; writing – original draft, L.Y., J.-M.M., J.R.S., J.W., and Y.S.M.; writing – review & editing, L.Y., J.-M.M., J.R.S., A.T., and J.W.; visualization, L.Y., J.-M.M., and J.R.S.; supervision, J.W. and S.X.; project administration, J.W.; funding acquisition, J.W.

DECLARATION OF INTERESTS

L.Y., J.-M.M., J.R.S., and J.W. are among the inventors of a provisional patent application related to this work.

Received: April 22, 2021
Revised: May 31, 2021
Accepted: June 9, 2021
Published: July 13, 2021

REFERENCES

1. Shi, Q., Dong, B., He, T., Sun, Z., Zhu, J., Zhang, Z., and Lee, C. (2020). Progress in wearable electronics/photonics—moving toward the era of artificial intelligence and internet of things. InfoMat *2*, 1131–1162.

2. Bandodkar, A.J., Lee, S.P., Huang, I., Li, W., Wang, S., Su, C.-J., Jeang, W.J., Hang, T., Mehta, S., Nyberg, N., et al. (2020). Sweat-activated biocompatible batteries for epidermal electronic and microfluidic systems. Nat. Electron. *3*, 554–562.

3. Yu, Y., Nassar, J., Xu, C., Min, J., Yang, Y., Dai, A., Doshi, R., Huang, A., Song, Y., Gehlhar, R., et al. (2020). Biofuel-powered soft electronic skin with multiplexed and wireless sensing for human-machine interfaces. Sci. Robot. *5*, eaaz7946.

4. Chen, J., Huang, Y., Zhang, N., Zou, H., Liu, R., Tao, C., Fan, X., and Wang, Z.L. (2016). Micro-cable structured textile for simultaneously harvesting solar and mechanical energy. Nat. Energy *1*, 16138.

5. Song, Y., Min, J., Yu, Y., Wang, H., Yang, Y., Zhang, H., and Gao, W. (2020). Wireless battery-free wearable sweat sensor powered by human motion. Sci. Adv. *6*, eaay9842.

6. Grattieri, M., and Minteer, S.D. (2018). Self-powered biosensors. ACS Sens *3*, 44–53.

7. Wu, W., and Haick, H. (2018). Materials and wearable devices for autonomous monitoring of physiological markers. Adv. Mater. *30*, e1705024.

8. Zhao, J., Lin, Y., Wu, J., Nyein, H.Y.Y., Bariya, M., Tai, L.C., Chao, M., Ji, W., Zhang, G., Fan, Z., and Javey, A. (2019). A fully integrated and self-powered smartwatch for continuous sweat glucose monitoring. ACS Sens *4*, 1925–1933.

9. Song, Y., Mukasa, D., Zhang, H., and Gao, W. (2021). Self-powered wearable biosensors. Acc. Mater. Res. *2*, 184–197.

10. Yin, L., Kim, K.N., Lv, J., Tehrani, F., Lin, M., Lin, Z., Moon, J.M., Ma, J., Yu, J., Xu, S., and Wang, J. (2021). A self-sustainable wearable multi-modular E-textile bioenergy microgrid system. Nat. Commun. *12*, 1542.

11. Wen, D.-L., Deng, H.-T., Liu, X., Li, G.-K., Zhang, X.-R., and Zhang, X.-S. (2020). Wearable multi-sensing double-chain thermoelectric generator. Microsyst. Nanoeng. *6*, 1–13.

12. Bandodkar, A.J., You, J.-M., Kim, N.-H., Gu, Y., Kumar, R., Mohan, A.M.V., Kurniawan, J., Imani,

S., Nakagawa, T., Parish, B., et al. (2017). Soft, stretchable, high power density electronic skin-based biofuel cells for scavenging energy from human sweat. Energy Environ. Sci. *10*, 1581–1589.

13. Jeerapan, I., Sempionatto, J.R., and Wang, J. (2020). On-body bioelectronics: wearable biofuel cells for bioenergy harvesting and self-powered biosensing. Adv. Funct. Mater. *30*, 1906243.

14. Siegel, J.A., Gilders, R.M., Staron, R.S., and Hagerman, F.C. (2002). Human muscle power output during upper- and lower-body exercises. J. Strength Cond. Res. *16*, 173–178.

15. Taylor, N.A., and Machado-Moreira, C.A. (2013). Regional variations in transepidermal water loss, eccrine sweat gland density, sweat secretion rates and electrolyte composition in resting and exercising humans. Extrem. Physiol. Med. *2*, 4.

16. Lin, S., Wang, B., Zhao, Y., Shih, R., Cheng, X., Yu, W., Hojaiji, H., Lin, H., Hoffman, C., Ly, D., et al. (2020). Natural perspiration sampling and in situ electrochemical analysis with hydrogel micropatches for user-identifiable and wireless chemo/biosensing. ACS Sens *5*, 93–102.

17. Nagamine, K., Mano, T., Nomura, A., Ichimura, Y., Izawa, R., Furusawa, H., Matsui, H., Kumaki, D., and Tokito, S. (2019). Noninvasive sweat-lactate biosensor Emplsoying a hydrogel-based touch pad. Sci. Rep. *9*, 10102.

18. Choi, J., Xue, Y., Xia, W., Ray, T.R., Reeder, J.T., Bandodkar, A.J., Kang, D., Xu, S., Huang, Y., and Rogers, J.A. (2017). Soft, skin-mounted microfluidic systems for measuring secretory fluidic pressures generated at the surface of the skin by eccrine sweat glands. Lab Chip *17*, 2572–2580.

19. Peng, R., Sonner, Z., Hauke, A., Wilder, E., Kasting, J., Gaillard, T., Swaille, D., Sherman, F., Mao, X., Hagen, J., et al. (2016). A new oil/membrane approach for integrated sweat sampling and sensing: sample volumes reduced from μL's to nL's and reduction of analyte contamination from skin. Lab Chip *16*, 4415–4423.

20. Lloyd, D.P.C. (1959). Secretion and reabsorption in sweat glands. Proc. Natl. Acad. Sci. USA *45*, 405–409.

21. Yoshihuku, Y., and Herzog, W. (1990). Optimal design parameters of the bicycle-rider system for maximal muscle power output. J. Biomech. *23*, 1069–1079.

22. Williams, K.R., and Cavanagh, P.R. (1983). A model for the calculation of mechanical power during distance running. J. Biomech. *16*, 115–128.

23. Rich, M., Mendecki, L., Mensah, S.T., Blanco-Martinez, E., Armas, S., Calvo-Marzal, P., Radu, A., and Chumbimuni-Torres, K.Y. (2016). Circumventing traditional conditioning protocols in polymer membrane-based ion-selective electrodes. Anal. Chem. *88*, 8404–8408.

24. Bandodkar, A.J., Gutruf, P., Choi, J., Lee, K., Sekine, Y., Reeder, J.T., Jeang, W.J., Aranyosi, A.J., Lee, S.P., Model, J.B., et al. (2019). Battery-free, skin-interfaced microfluidic/electronic systems for simultaneous electrochemical, colorimetric, and volumetric analysis of sweat. Sci. Adv. *5*, eaav3294.

25. Jin, X., Bandodkar, A.J., Fratus, M., Asadpour, R., Rogers, J.A., and Alam, M.A. (2020). Modeling, design guidelines, and detection limits of self-powered enzymatic biofuel cell-based sensors. Biosens. Bioelectron. *168*, 112493.

26. Sempionatto, J.R., Khorshed, A.A., Ahmed, A., De Loyola E Silva, A.N., Barfidokht, A., Yin, L., Goud, K.Y., Mohamed, M.A., Bailey, E., May, J., et al. (2020). Epidermal enzymatic biosensors for sweat vitamin C: toward personalized nutrition. ACS Sens *5*, 1804–1813.

27. Falk, M., Andoralov, V., Silow, M., Toscano, M.D., and Shleev, S. (2013). Miniature biofuel cell as a potential power source for glucose-sensing contact lenses. Anal. Chem. *85*, 6342–6348.

28. Jeerapan, I., Sempionatto, J.R., Pavinatto, A., You, J.M., and Wang, J. (2016). Stretchable biofuel cells as wearable textile-based self-powered sensors. J. Mater. Chem. A Mater. *4*, 18342–18353.

29. Tang, W., Yin, L., Sempionatto, J.R., Moon, J.M., Teymourian, H., and Wang, J. (2021). Touch-based stressless cortisol sensing. Adv. Mater. *33*, e2008465.

30. Kumar, R., Shin, J., Yin, L., You, J.M., Meng, Y.S., and Wang, J. (2017). All-printed, stretchable Zn-Ag2O rechargeable battery via hyperelastic binder for self-powering wearable electronics. Adv. Energy Mater. *7*, 1602096.

31. Sempionatto, J.R., Lin, M., Yin, L., De la Paz, E., Pei, K., Sonsa-Ard, T., de Loyola Silva, A.N., Khorshed, A.A., Zhang, F., Tostado, N., et al. (2021). An epidermal patch for the simultaneous monitoring of haemodynamic and metabolic biomarkers. Nat. Biomed. Eng. https://doi.org/10.1038/s41551-021-00685-1.